UCRL-12125

UNIVERSITY OF CALIFORNIA
Lawrence Radiation Laboratory
Livermore, California

Contract No. W-7405-eng-48

# PREDICTION OF FALLOUT FROM SUBSURFACE NUCLEAR DETONATIONS

Joseph B. Knox

October 14, 1964

Prepared for presentation at the 2nd AEC Conference on Radioactive Fallout from Nuclear Weapons Tests, November 3-6, 1964.

## DISCLAIMER

# PREDICTION OF FALLOUT FROM SUBSURFACE NUCLEAR DETONATIONS

Joseph B. Knox

Lawrence Radiation Laboratory, University of California

Livermore, California

October 14, 1964

## ABSTRACT

A numerical simulation model has been developed for the prediction of fallout from subsurface nuclear detonations that produce craters through spall and the action of the cavity gas. The physical processes modeled are atmospheric transport, lateral eddy diffusion, and gravitational sedimentation of radioactive particulates. This "cratering fallout model" is normalized to the observed external gamma dose rate fields of the Sedan (100-kt) and Danny Boy (0.43-kt) cratering events conducted at the Nevada Test Site. Calculations of the fallout patterns for additional events, used for testing the prediction capability of the cratering fallout model, indicate that the model gives estimates of the external gamma dose rate at H + 1 hours with a maximum error of a factor of 2 to 3 in the gamma dose rate versus distance along the hot line of the pattern.

## I. INTRODUCTION

During the past few years, a small but continuing effort has been expended in developing a model for predicting fallout from subsurface nuclear detonations. In this report, we (a) summarize the experience in predicting fallout from surface bursts that is transferable to the construction of a fallout model for subsurface detonation, (b) describe the development of the fallout

model for subsurface nuclear detonations (the cratering fallout model), (c) illustrate by means of an independent test case the predictive capability of the model, and (d) discuss some of the problems associated with the prediction of fallout from row-charge subsurface nuclear detonations. This paper is limited to research or development in which the investigator has been personally involved within the Plowshare Program of the Lawrence Radiation Laboratory.

## II. THE CRATERING FALLOUT MODEL

### A. Basis of Model Construction

In order to predict the area affected by radioactive fallout from a subsurface detonation of a nuclear explosive, and to predict the gross external gamma dose rate in the surface fallout pattern, we need knowledge of the following:

1. The height of the base and top, and the radius, of each radioactive cloud (i. e., the main cloud and base surge cloud) formed by the detonation at the time the clouds cease to rise in the atmosphere. (This time is defined as the time of cloud stabilization.) The cloud heights are prescribed in terms of height above surface zero.

2. The total yield of the explosive, $W_T$, the fission yield of the explosive, $W_f$, the depth of burial of the explosive, z, the fraction of the fission-product gamma emitters expected to appear in the fallout pattern beyond the (estimated) radius of direct ejecta, $F_c$, and the equivalent fission yield gamma needed to simulate gamma dose from induced activities.

3. The activity-particle size distribution in the main cloud and the base surge, and the fraction of $F_c$ in each of these clouds.

4. The terminal fall velocity of the fallout particles (in still air) as a function of particle size and height in the atmosphere.

5. In a fallout calculation involving two clouds, main cloud and base surge, the calculation of the fallout pattern for each cloud is done separately. The total surface fallout pattern of the event is found by summing the patterns from the base surge and main clouds. Thus, the time and space prediction of the horizontal wind at the level of each cloud top is required, along with the specification of the wind-shear tangential and normal to the wind for the layer through which particles fall.

6. The effect of horizontal eddy diffusion on the growth of the horizontal radius of the disks of radioactive particles as the disks fall earthward. (The initial debris cloud is subdivided into disks of debris in the model as a function of initial height in the cloud and particle size.)

The above information provides the simplest but still adequate basis for constructing a cratering fallout model. In addition to this information, we assume that the fission product radioactivity is unfractionated and that 1 kiloton of unfractionated fission products spread uniformly over 1 square mile corresponds to an (H + 1)-hour dose rate of 3380 R/hr at a height of 3 feet above an infinite plane [Higgins, 1963]. This normalization constant of 3380 R/hr is corrected for terrain shielding by a factor of 0.8.

Certain atmospheric processes or effects have been neglected in developing the cratering fallout model, just as these same effects were neglected in developing the land surface-burst fallout model [Knox, 1964a]:

7. The effect of synoptic-scale vertical motions on the vertical displacement of the falling disk of particles.

8. The effect of the mean divergence of the horizontal wind on the radius of the disk of falling particles during descent.

9. The effect of vertical eddy diffusion.

10. The time from detonation to cloud stabilization.

11. The development of subsynoptic-scale wind systems.

12. Changes in time and space of the shear tangential and normal to the horizontal wind at cloud top level.

13. The effect of water products of condensation on the size and fall rate of radioactive particles.

We consider now, more fully, items one through six.

## B. Fraction of Gamma Activity in the Close-In Pattern

In order to calculate the close-in fallout pattern from a subsurface detonation, the fraction of the gamma activity produced by the fission yield and appearing in the close-in fallout pattern $F_c$ must be known. To date, experimental data from Sedan, Teapot ESS, Jangle U, Neptune, and Jangle S (and other surface burst events) have provided a basis for estimating $F_c$. Integration of the measured fallout patterns for these events has been performed [Williamson, private communication, 1964] from the radius of direct throwout to the limit of the measured pattern, with results as shown in Table I.

Table I. Experimental $F_c$ data.

| Event | W, kt | z, ft | $F_c$ | Medium |
|---|---|---|---|---|
| Sedan | 100 | 635 | ~0.10 | Alluvium (A) |
| Teapot ESS | 1.2 | 67 | 0.46 | A |
| Jangle U | 1.2 | 17 | 0.64 | A |
| Neptune | 0.115 | 100 | 0.005 | Tuff |
| Jangle S | 1.2 | 0 | 0.50 | A |
| Danny Boy | 0.43 | 109 | 0.04 | Basalt |
| Blanca | 19 | 835 | 0.0005 | Tuff |

These $F_c$ calculations were performed assuming a normalization constant of 3380 R/hr per kt of fission yield per square mile at (H + 1) hours and a terrain shielding factor of 0.8. The graphical presentation of $F_c$ as a function of $z/W^{1/3}$ is shown in Fig. 1. In constructing the experimental $F_c$ curve, we have been guided by:

1. An asymptote of $F_c = 0.50$ for $z = 0$, suggested by Jangle S data in the Table I and supported by previous work [Nordyke and Wray, 1964].

2. An asymptote of no dynamic venting for $z/W^{1/3} = 330$ ft/kt$^{1/3}$ supported by experimental evidence [Higgins, private communication, 1964] and by studies of containment physics [Knox, unpublished Internal LRL Memorandum, 1963].

It should be noted that the value of $F_c$ (estimated by pattern integration) for the Sedan event departs considerably from the curve fitted to the whole sample of $F_c$ data. This departure could arise because of an $F_c$ yield dependency that is inadequately known at this time. In the absence of knowledge of such an $F_c$ dependency, $F_c$ estimates made from the $F_c$ curve in Fig. 1 for high-yield cratering events (of the order of 100 kt and above) should be considered as uncertain by a factor of 2. It should be further stated that $F_c$ estimates derived from Fig. 1 tacitly assume that the nuclear explosive is fully tamped and that no additives for fission-product gamma radiation suppression have been placed around the explosive.

It should also be mentioned that the maximum value of $F_c$ (0.75 at $z/W^{1/3} \approx 30$) occurs at very nearly the same value of $z/W^{1/3}$ as the maximum base surge radius (crosswind) in a neutral atmosphere, reported earlier [Knox and Rohrer, 1963]. The author believes that this coincidence of maxima at $z/W^{1/3} \approx 30$ is physically consistent.

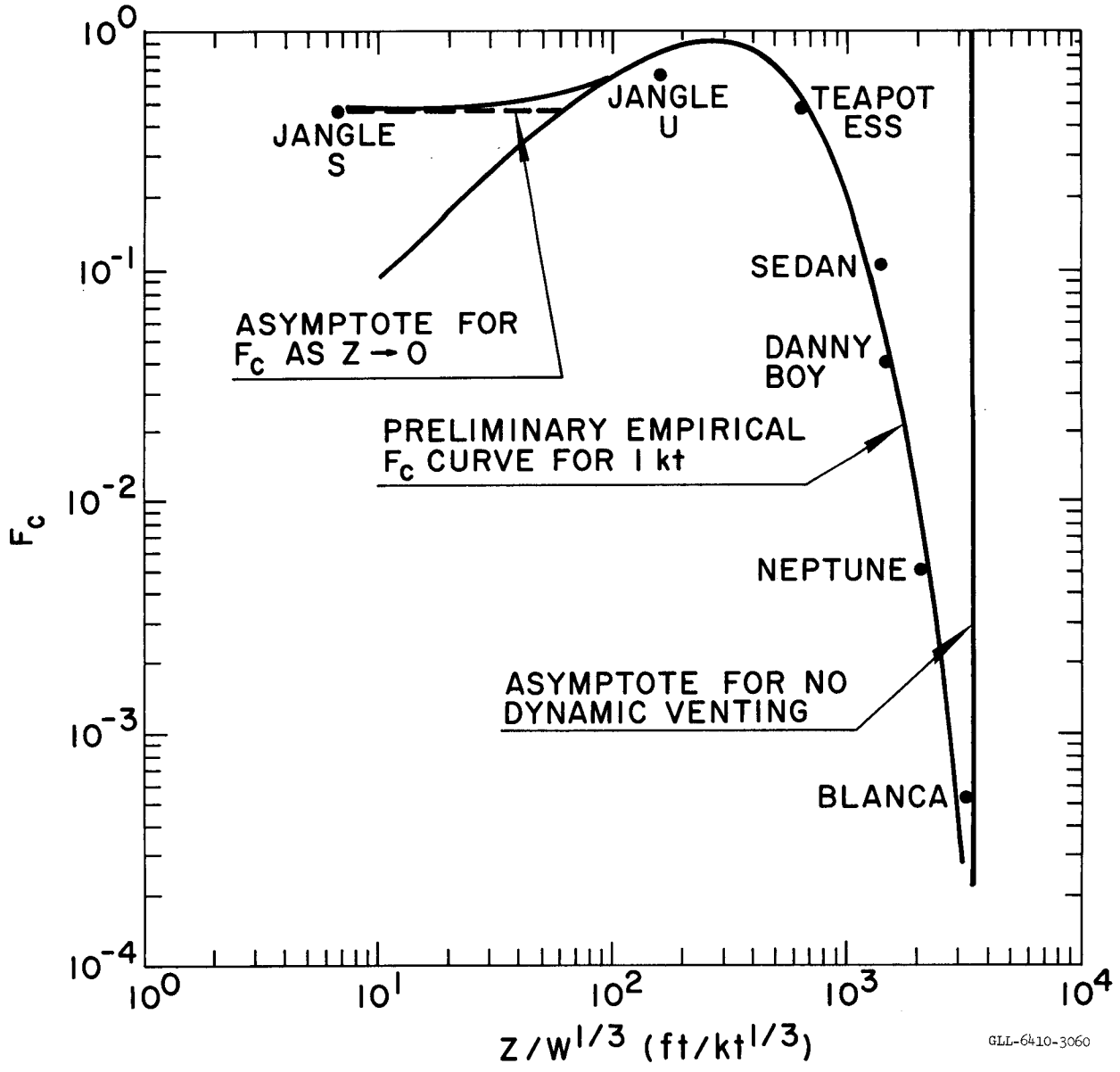


Fig. 1. Fraction of the gamma activity appearing in the close-in fallout pattern.

## C. Cloud Geometries

The geometrical definition of the cloud top, base, and radius for the main cloud and base surge cloud at the time of cloud stabilization is shown in Fig. 2. In addition to the definitions given in Fig. 2, the height of the base of the main cloud is defined as being equal to the height of the base surge cloud top $H_b$ in the model.

Evidence suggests that the geometry of these two clouds at the time of stabilization is a function of the total explosive yield, the material in which the detonation occurs, depth of burial of the explosive, and the meteorological conditions existing during the development of the clouds. [Knox and Rohrer, 1963]. At present, the cloud geometry parameters ($R_b$, $H_b$, $R_m$, $H_m$) must be evaluated experimentally as functions of total yield and depth of burial. Reasonable samples of experimental data exist for alluvium and basalt materials. An example of one of the most useful summaries of cloud geometry data for alluvium is shown in Fig. 3b-g* [W. Day, U. S. Army Corps of Engineers Nuclear Cratering Group, LRL, private communication, 1964]. Day's summary utilizes all of the known cloud geometry data from high explosive and nuclear explosive detonations conducted by the U. S. Atomic Energy Commission in alluvium and basalt. Implicit in Day's summary is the assumption that a high explosive and nuclear explosive detonated in the same material at identical depths of burial and under similar meteorological conditions produce the same cloud geometries.

---

*Figure 3a is a computational aid to the acquisition of input to Fig. 3b-g. In these figures, DOB denotes depth of burial, and $D_a$ denotes the depth of apparent crater.

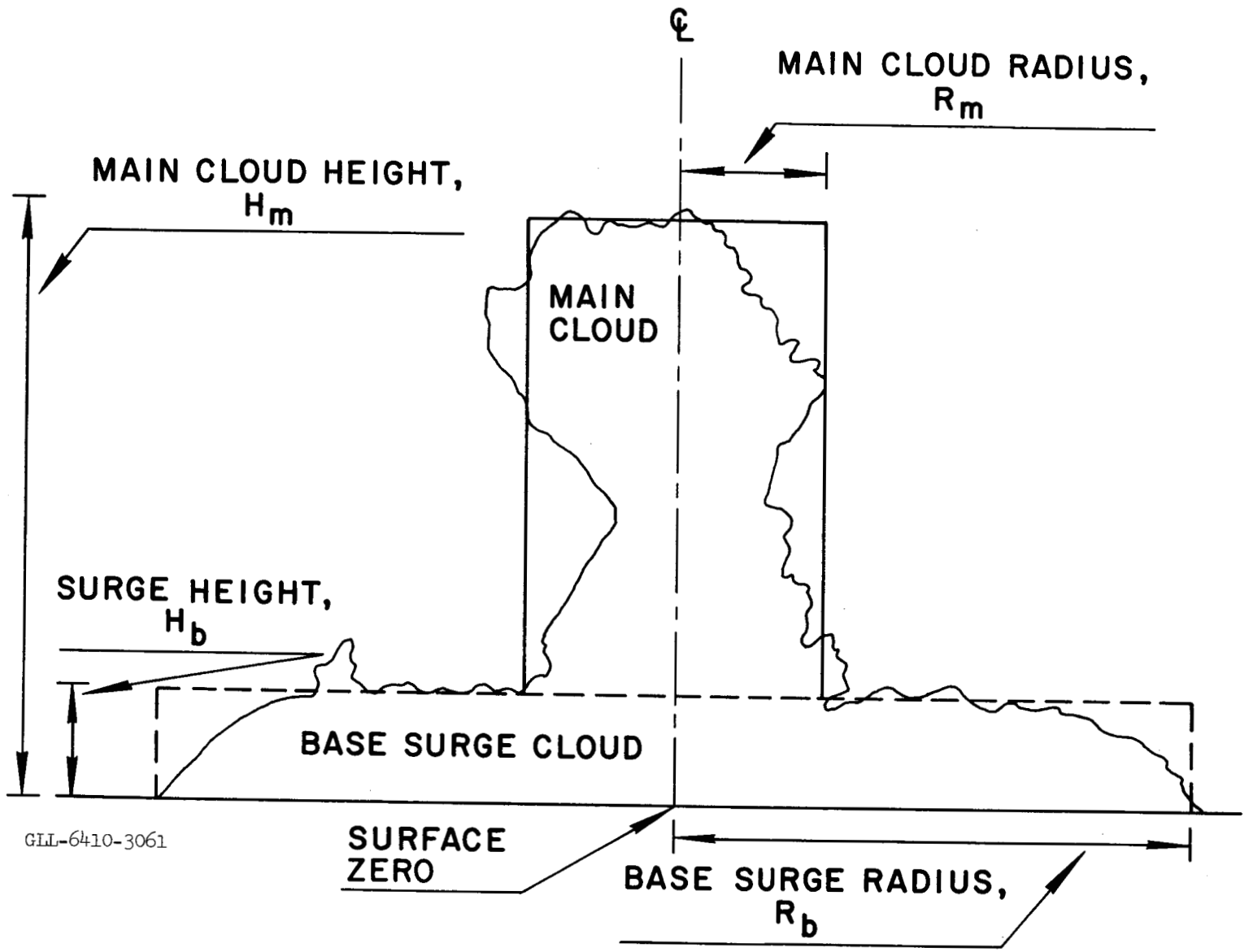


Fig. 2. Definition of cloud dimensions and symbols.

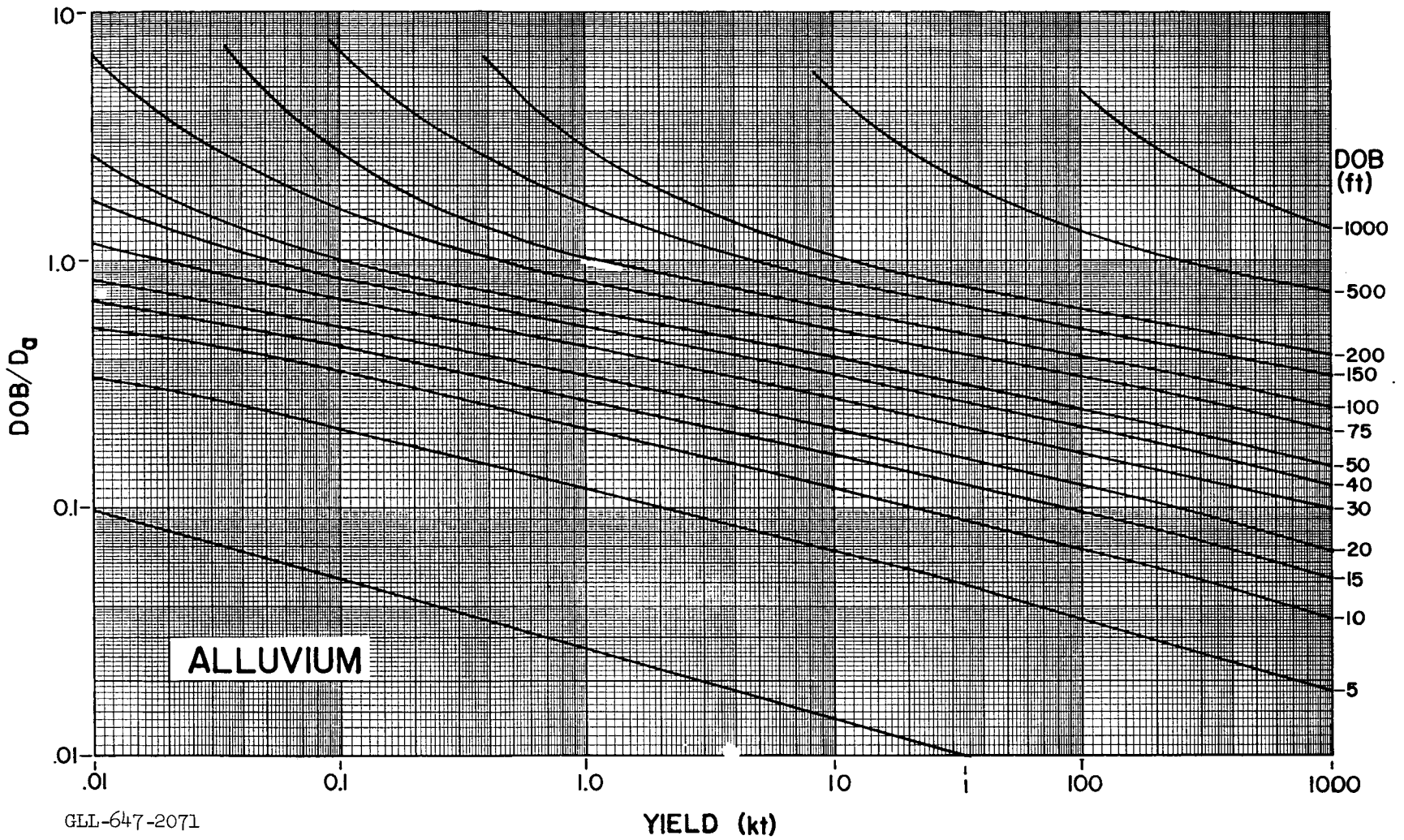


Fig. 3a. Computational aid to the acquisition of input data to the cloud dimension graphs, Fig. 3b-g.

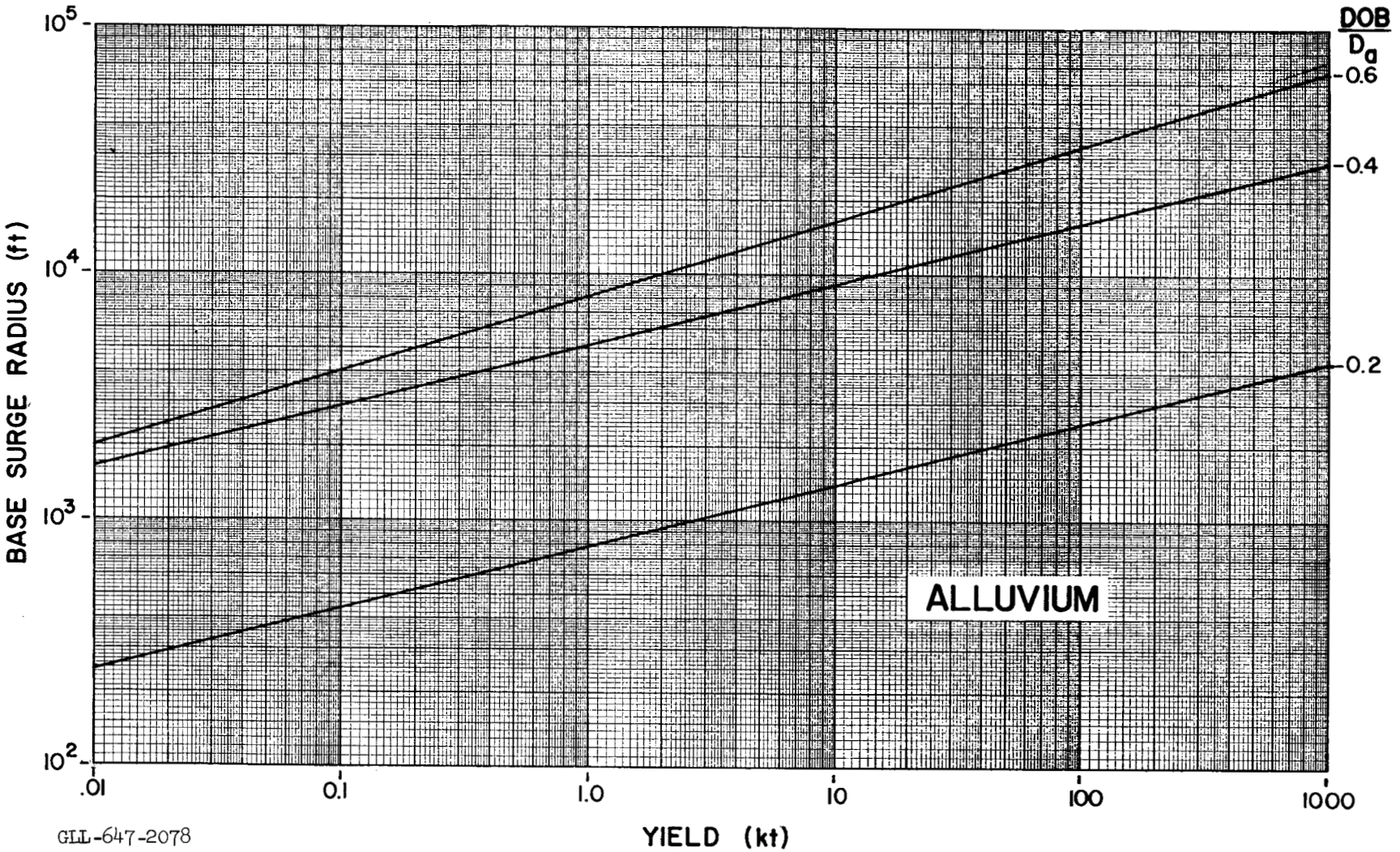


Fig. 3b. Base surge radius as a function of yield (total) and the parameter DOB/$D_a$ (alluvium).

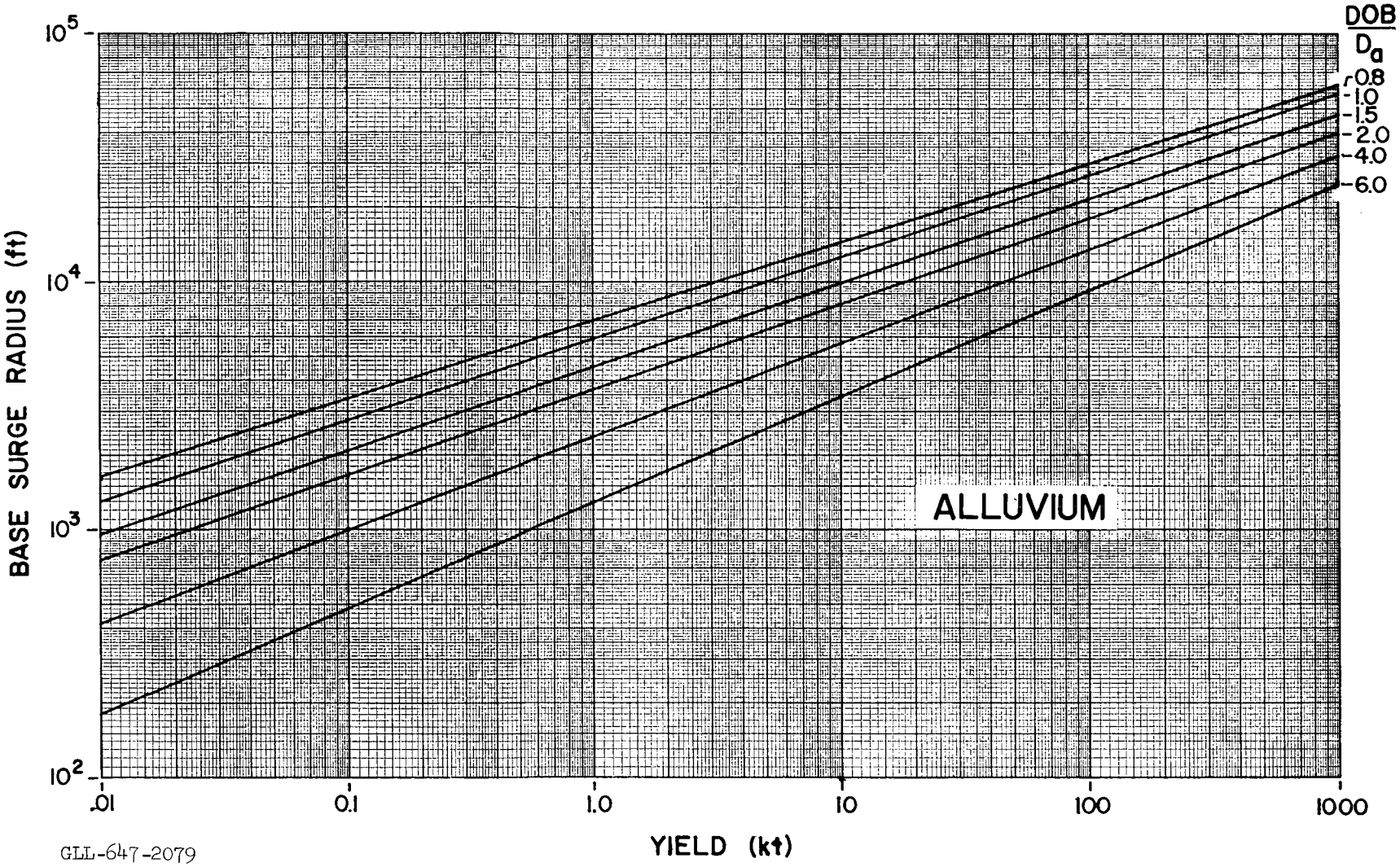


Fig. 3c. Base surge radius as a function of yield (total) and the parameter DOB/$D_a$ (alluvium).

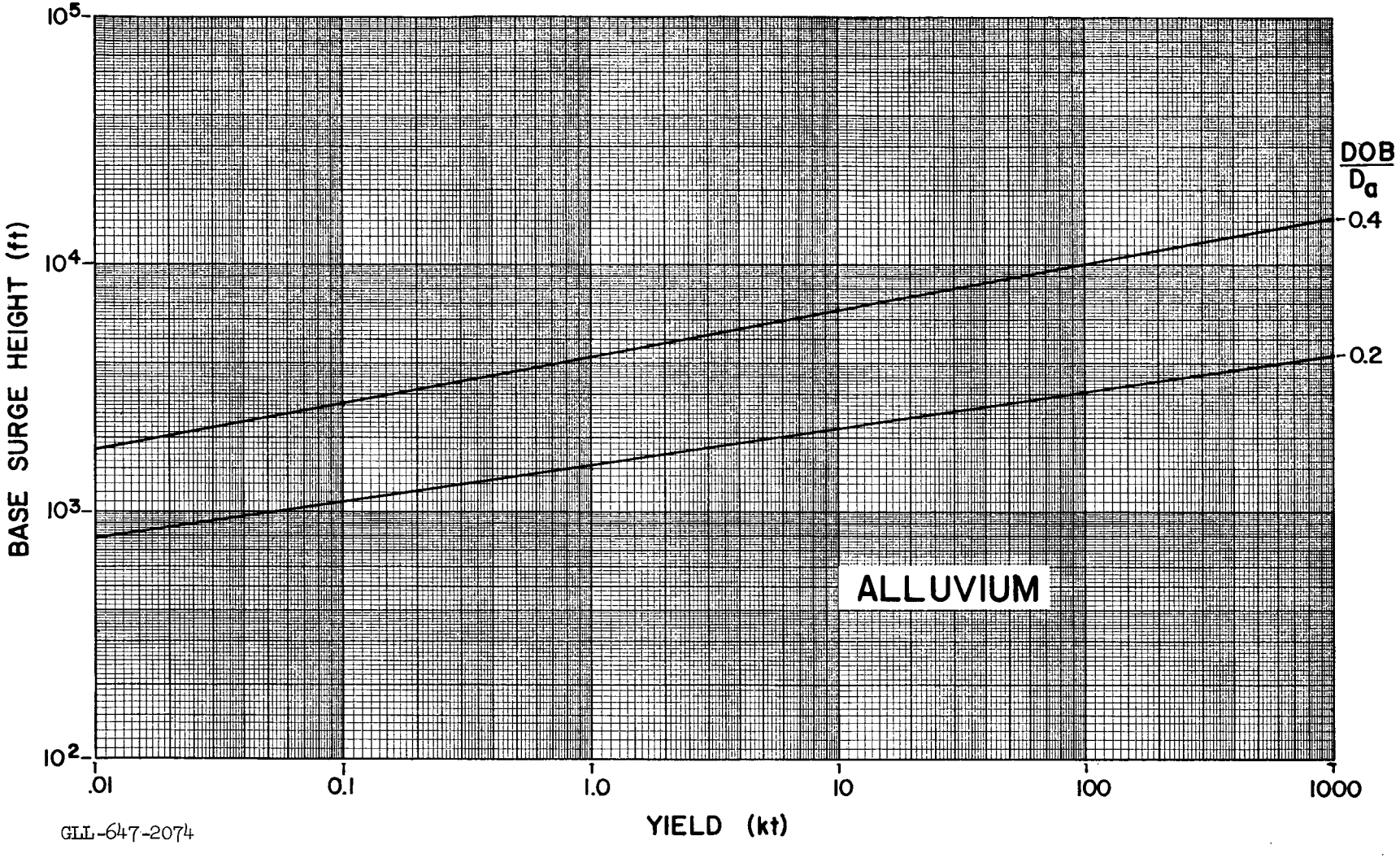


Fig. 3d. Base surge height as a function of the yield (total) and the parameter $DOB/D_a$ (alluvium).

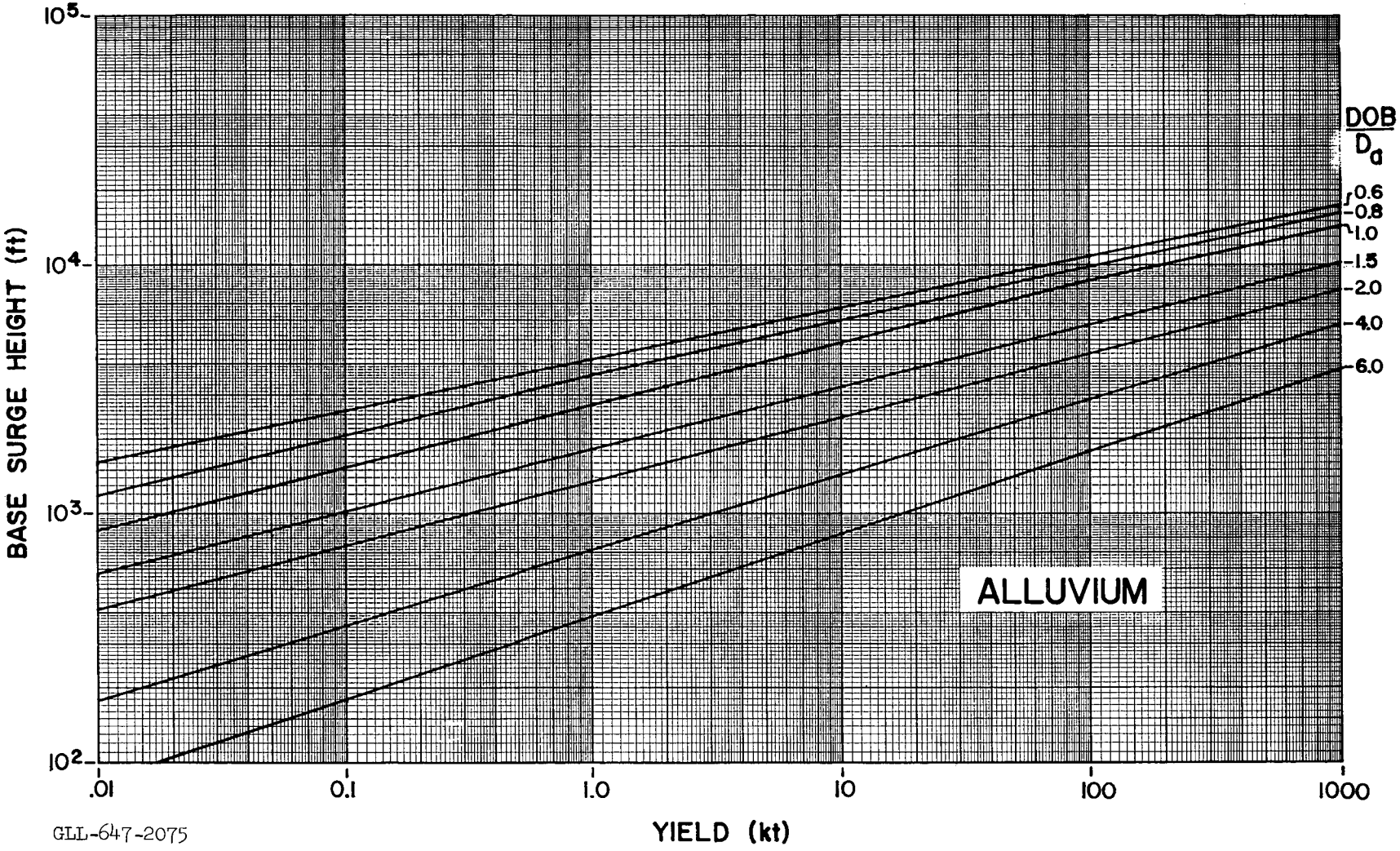


Fig. 3e. Base surge height as a function of the yield (total) and the parameter $DOB/D_a$ (alluvium).

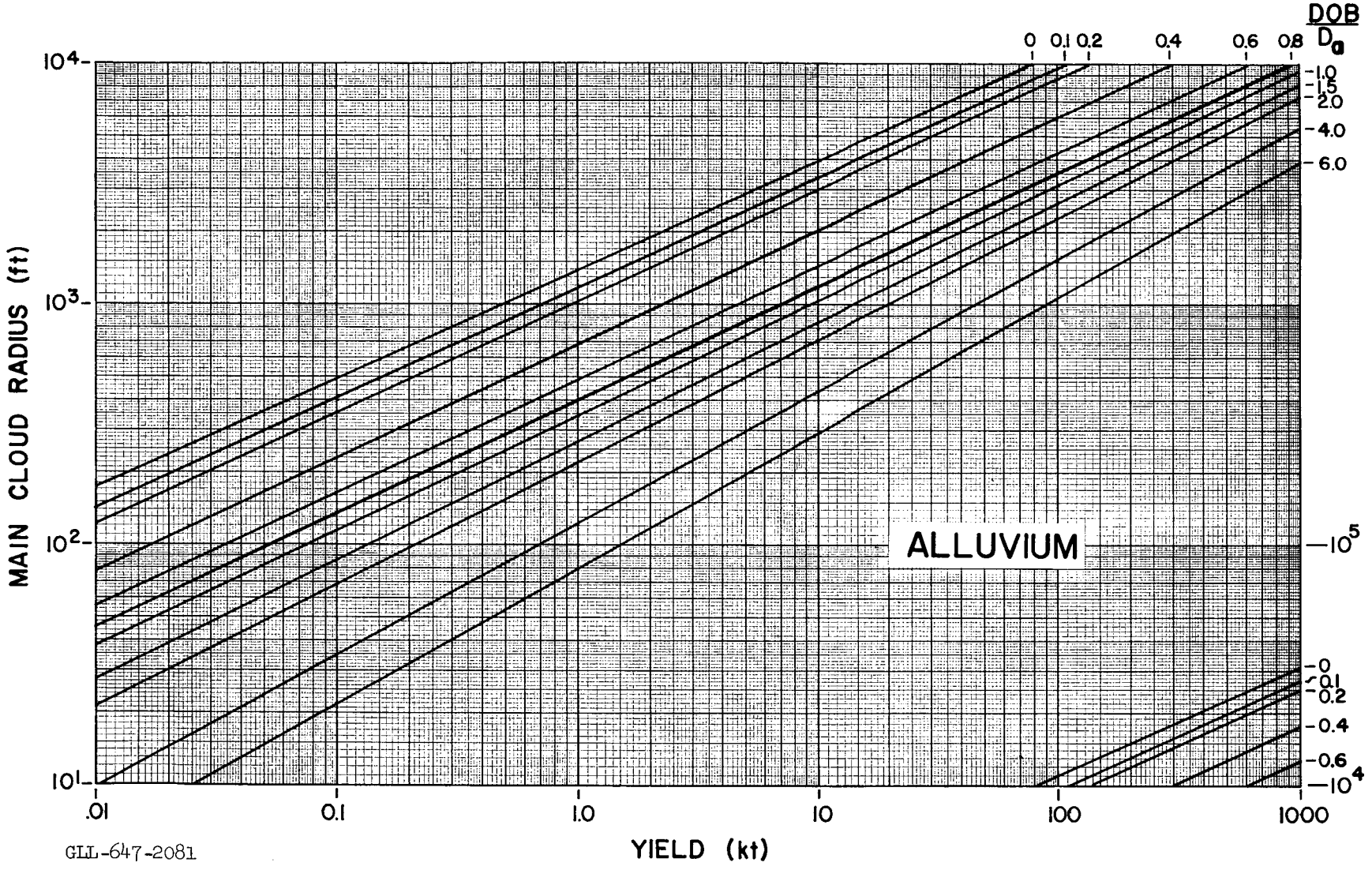


Fig. 3f. Main cloud radius as a function of the yield (total) and the parameter DOB/$D_a$ (alluvium).

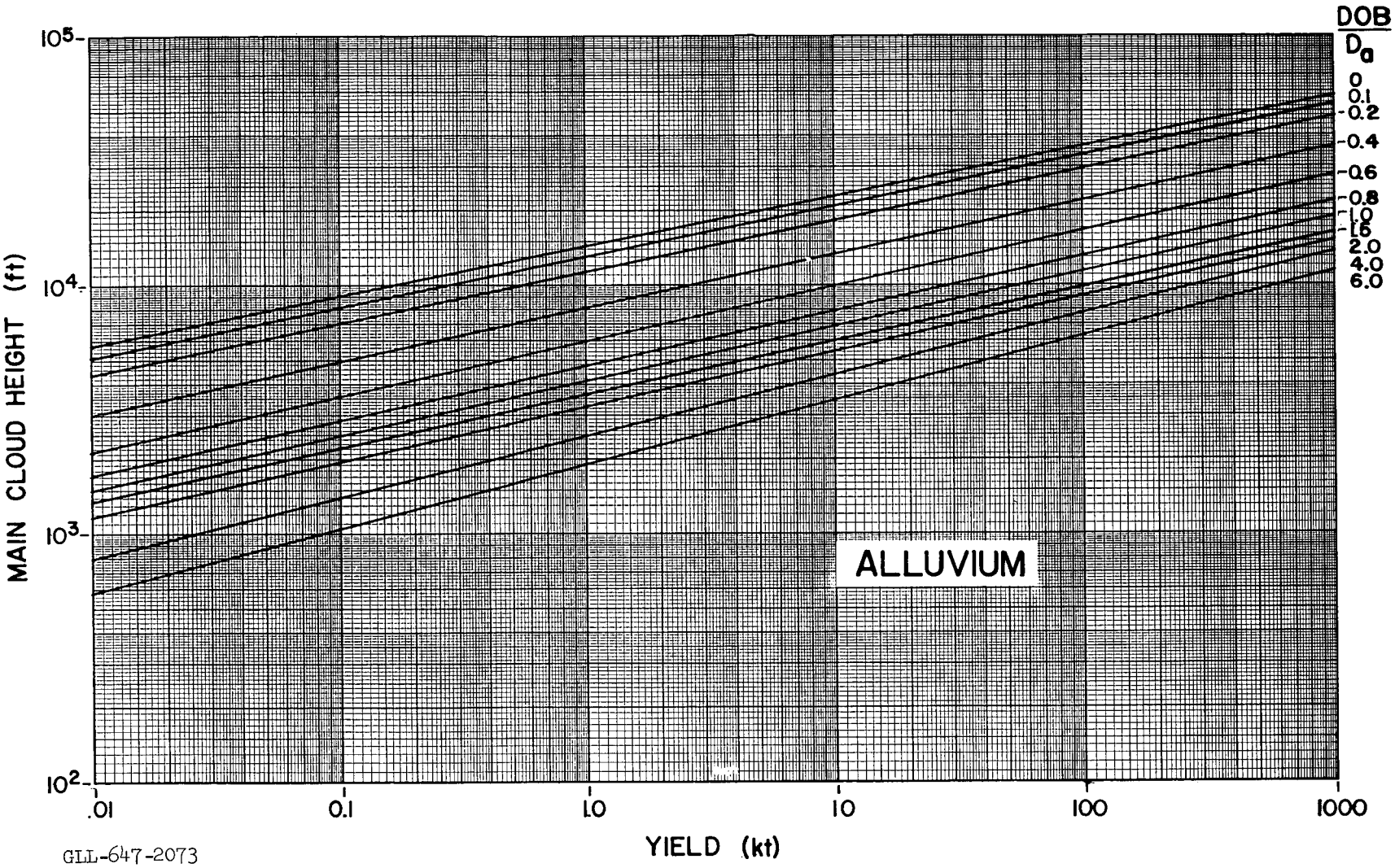


Fig. 3g. Main cloud height as a function of the yield (total) and the parameter DOB/$D_a$ (alluvium).

## D. Activity-Particle Size Distributions

In a typical subsurface nuclear detonation in alluvium, two clouds are formed. The main cloud is composed mostly of vented cavity gas and particulates (originating either from condensation or injection and entrainment of soil). The base surge cloud is composed of ejecta and suspended fine particulates. For a nuclear cratering shot in alluvium, it is assumed that 80% of the $F_c$ gamma activity is in the main cloud and 20% in the base surge cloud. The $0.8\ F_c$ main cloud activity is assumed to be subdivided between two log-normal activity-particle size distributions. The first activity-particle size distribution contains the activity $0.8\, w_m(1)F_c$, and is characterized by the mean $\ln \bar{r}_m(1)$ and the standard deviation $\sigma_m(1)$. The second activity-particle size distribution contains the activity $0.2\, w_m(2)F_c$, and is characterized by the mean $\ln \bar{r}_m(2)$ and the standard deviation $\sigma_m(2)$. The activity of the first distribution is assumed to be homogeneously mixed through the whole main cloud, while that of the second distribution is assumed to be homogeneously mixed in the lower fifth of the cloud. A similar prescription of activity vs particle size is used for the base surge cloud. Figure 4 summarizes the parameters governing the activity-particle size distributions in the two clouds at the time of cloud stabilization. These parameters governing the activity-particle size distributions in the cratering fallout model have been determined by mathematical experimentation with the model in the recreation of the observed fallout patterns for the Sedan and Danny Boy events. Results of these calibration calculations will be discussed in a later section.

## E. Terminal Fall Velocity of Fallout Particles

The vertical fall velocities of the fallout particles are modeled as the terminal fall velocities of smooth spheres of density 2.5 g/cc in an I. C. A. O.

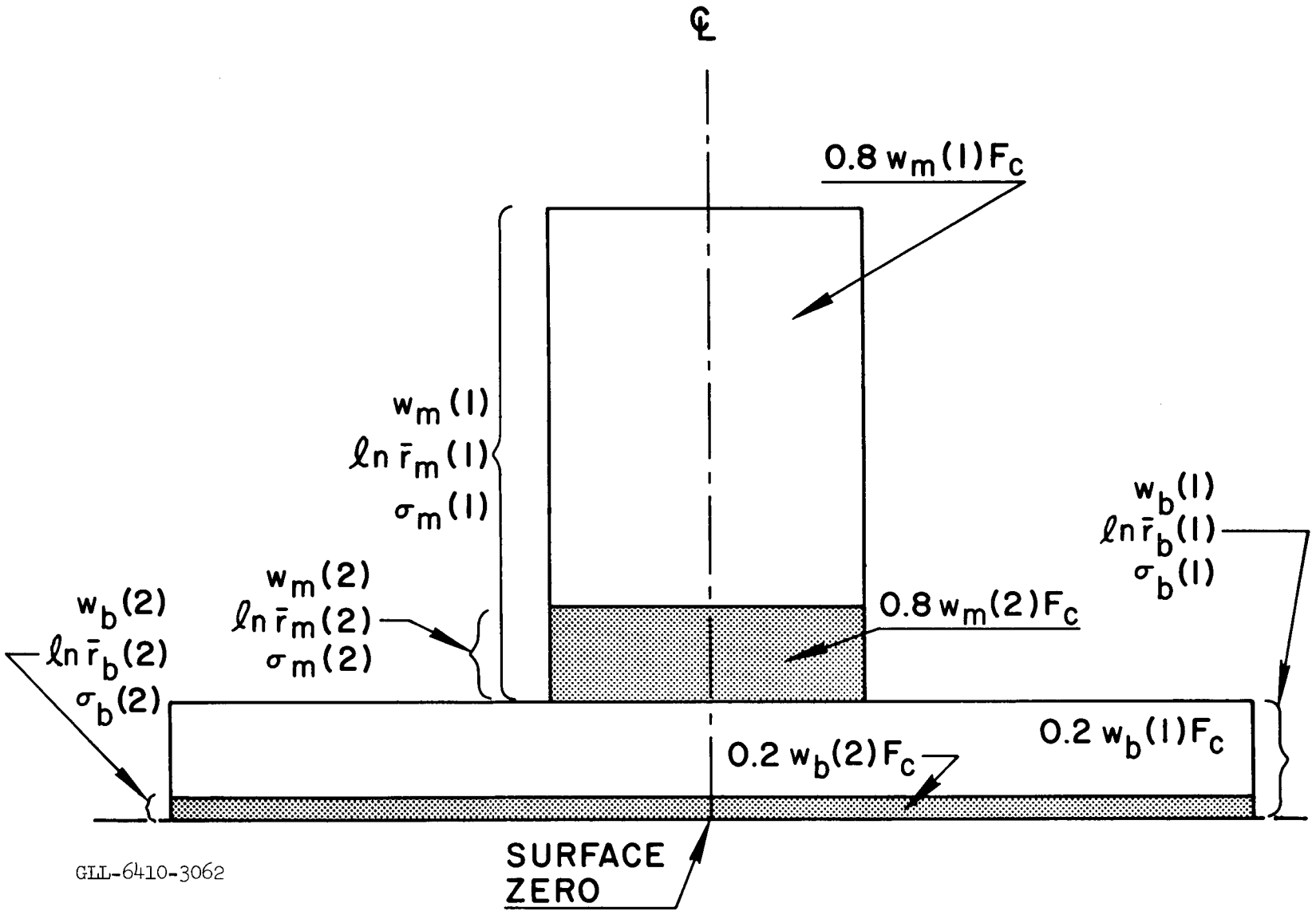


Fig. 4. Schematic drawing of an idealized cloud from a subsurface detonation showing spatial relationships of the activity-particle size distribution assumed in the model.

standard atmosphere as computed by McDonald [1960] for both the Stokes law region and the aerodynamic region (wherein the Reynolds number exceeds 1). If in reality some fallout particles are a cluster of small spheres attached to a large central particle, these complex particles are assumed to fall with the speed of the equivalent smooth spherical particle of the same mass. Experimental evidence has been obtained by Rapp and Sartor [1957] to support this assumption.

## F. Specification of the Horizontal Wind Field for the Model

The horizontal wind field that transports the debris disk centroids during their fall to the earth's surface may be specified in two ways in the cratering fallout model.

### Option 1. Idealized Wind Hodograph

If H denotes height above surface zero, then the horizontal wind $\underset{\sim}{v}_h$ at height H for a simple wind hodograph (see Fig. 5) is

$$\underset{\sim}{v}_h(H) = \underset{\sim}{v}_h(H_m)\,\frac{A(p)}{A(p_m)} - S(H_m - H)\underset{\sim}{n}$$

where

$\underset{\sim}{v}_h(H_m)$ can be specified as a steady state wind at the cloud top level $H_m$, or $\underset{\sim}{v}_h(H_m)$ can be specified as a function of time and space in either wind component form or by means of a stream function;

A(p) characterizes the wind shear component tangential to the horizontal wind at cloud top level and is evaluated from shot time winds (in a diagnostic fallout calculation) or from preshot wind information (for a predictive fallout calculation), and it is held constant in time for the period of fallout deposition;

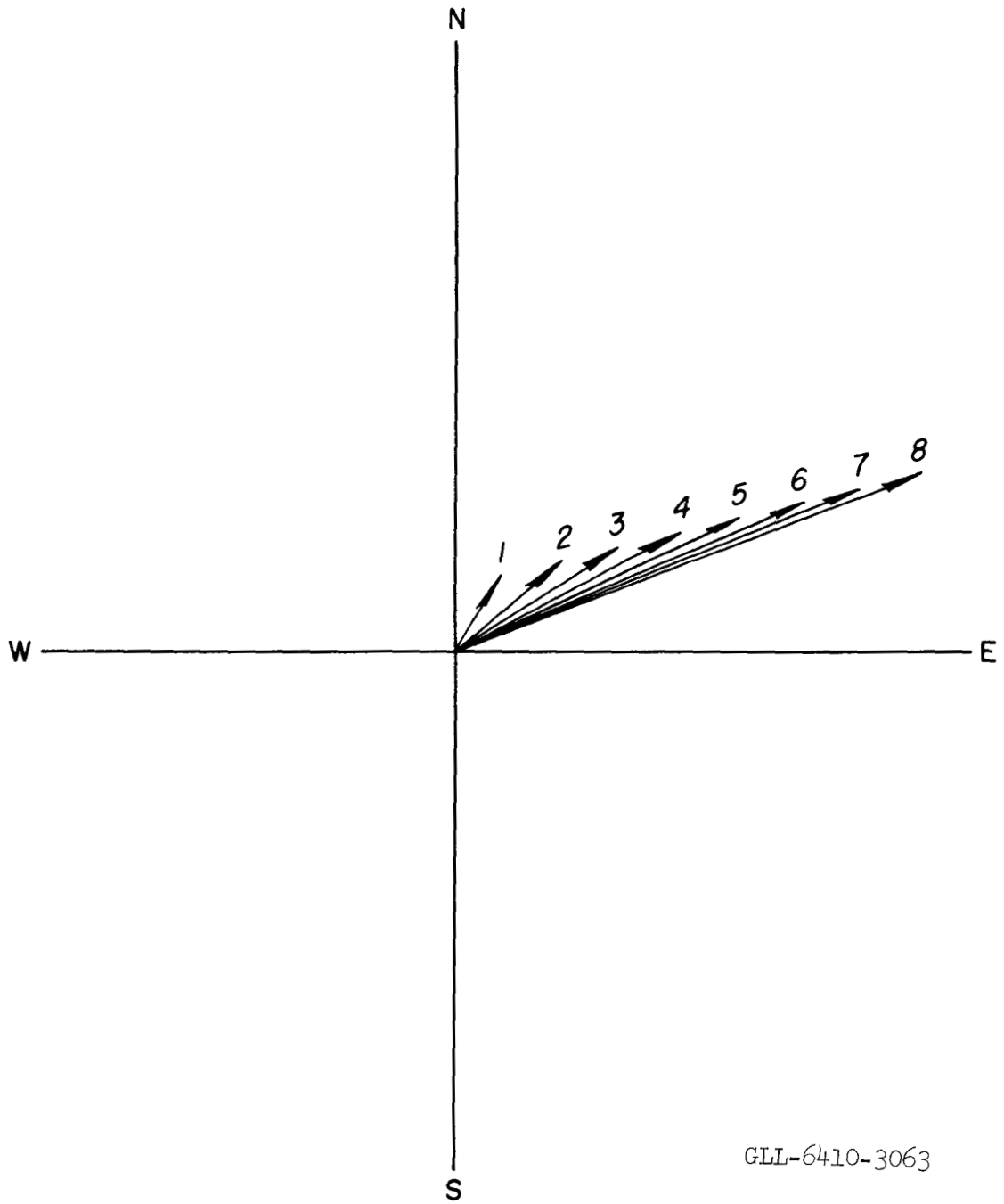


Fig. 5. Simple wind hodograph assumed in the model for wind specification (Option 1).

$A(p_m)$ is the value of $A(p)$ at cloud top level (normally it is set equal to 1);

S is the wind shear component normal to the horizontal wind at cloud top level, evaluated from shot time winds or preshot wind information (depending on the purpose of the fallout calculation) and held constant in time;

$\underset{\sim}{n}$ is the unit vector normal to $\underset{\sim}{v}_h(H_m)$ in a right-handed system;

p is the atmospheric pressure corresponding to H.

Option 2. Arbitrary Hodograph

In Option 2 the horizontal wind can be specified in wind component form for as fine a vertical interval as desired or for which wind information exists.

## G. Debris Disk Radius as a Function of Time

To estimate the radius of a debris disk expanding by horizontal eddy diffusion during its fall to earth, we propose that the disk radius as a function of time $R_e(t)$ be represented by

$$R_e(t) = (R_{e,0} + 2Dt')^{1/2}$$

where t' is the distance traveled by the disk centroid divided by the mean horizontal wind speed in the layer through which the disk has settled, $R_{e,0}$ is the debris disk radius at time of stabilization, and D is the horizontal eddy diffusion coefficient [Knox, 1964a]. The diffusion coefficient D is estimated as the Richardson's diffusion coefficient $0.2 \times (l)^{4/3}$ where $l$ is the standard deviation of the position of the particles (in the disk) from the disk centroid. Since $l$ is poorly known in nuclear debris clouds, it is usually set equal to $R_{e,0}$ or $2R_{e,0}$ if accelerated relative diffusion is to be approximated in the fallout model.

## H. Physical Processes Simulated in the Model

The principal physical or meteorological processes simulated by the cratering fallout model are: (a) the transport of the debris disks by the mean wind in the layer through which the disks are falling, (b) the relative advection of the debris disks by the horizontal wind field containing both speed and directional shear, and (c) lateral eddy diffusion which expands the disks falling earthward.

The first two processes are simulated by calculating the transport of the disk centroids by the ambient horizontal wind field during the disk's earthward fall until the disk centroid is on the ground surface, using either Option 1 or 2 for the horizontal wind specification. The result of this calculation is the position vector from surface zero to the predicted ground position of each disk centroid and the time of arrival at the ground surface of each disk. Process (c), above, is modeled by the expression for $R_e(t)$ which estimates the debris disk radius at the time of arrival of the disk centroid on the ground surface.

The debris disks tracked earthward are defined as follows: In each cloud (main cloud and base surge cloud) 11 disks of particle size $r_I$ are defined at each isobaric surface $p_p$ such that

$$\ln r_I = \ln r_L - \frac{I}{10}(\ln r_L - \ln r_s)$$

where

$I = 0, 1, 2, \ldots, 10,$

$r_L$ is the radius of the largest particle modeled in the cloud,

$r_S$ is the radius of the smallest particle modeled in the cloud,

$p_p = p_B - \frac{P}{10}(p_B - p_m)$ and $P = 0, 1, 2, \ldots, 10,$

$p_B$ is the pressure at the base of the cloud at the time of cloud stabilization,

$p_m$ is the pressure at the top of the cloud at the time of cloud stabilization.

The (H +1)-hour external gamma dose rate (for a height 3 ft above an infinite plane) is calculated using the method of Batten, Inglehart, and Rapp [1960] modified to account for the effect of normal shear S and lateral eddy diffusive disk growth.

The following quantities are calculated in the model and are output in the indicated modes*:

| | Printout | CRT display |
|---|---|---|
| (a) Position of surface zero | | x |
| (b) Dose rate (H + 1) at the predicted ground position of each disk centroid for each cloud | x | |
| (c) The predicted ground position of each disk centroid for each cloud | x | x |
| (d) The envelope containing the area affected by the fallout from each cloud | | x |
| (e) The time of beginning and end of fallout deposition at each ground position centroid for each cloud | x | |
| (f) The isopleths of the (H + 1)-hour dose rate for any specified interval of dose rate (each contributing cloud and total pattern) | | x |
| (g) The (H + 1)-hour dose rate as a function of distance along the hot line (each cloud and total pattern) | | x |

*For a two-cloud nuclear cratering fallout problem about 0.25 min of 7094 time is required for the calculations, and 2.4 min of LARC time is required for the CRT displays indicated above.

## III. DIAGNOSTIC CALCULATION FOR SEDAN

In order to calibrate the cratering fallout model on the Sedan event, the observed shot time winds, the observed cloud geometry of the main cloud and base surge cloud, the estimated $F_c$ = 10%, and the appropriate fission yield were input to the model. A first " guess" of the 12 activity-particle size parameters, discussed in Section IV, was also input to the model. The main cloud was assumed to contain 80% of $F_c$, the base surge cloud 20%. By mathematical experimentation, the parameters governing the activity-particle size distributions have been determined from the observed Sedan gross gamma fallout pattern. The values of these parameters are as follows:

$$w_m(1) = w_b(1) = 0.9$$
$$w_m(2) = w_b(2) = 0.1$$
$$\ln \bar{r}_m(1) = \ln \bar{r}_b(1) = 2.9$$
$$\ln \bar{r}_m(2) = \ln \bar{r}_b(2) = 5.0$$
$$\sigma_m(1) = \sigma_b(1) = 0.69$$
$$\sigma_m(2) = \sigma_b(2) = 0.59$$

Figure 6 shows the calculated and the observed gamma dose rate* (at H + 1) from fission products vs distance along the hot line for the Sedan event.

## IV. DIAGNOSTIC CALCULATION FOR DANNY BOY

The Danny Boy event was a 0.42-kt nuclear cratering detonation emplaced at a depth of 109 ft in dry basalt. The observed gamma fallout pattern for Danny Boy has been published [Nordyke and Wray, 1964]. By mathematical experimentation with the cratering fallout model, we can adjust the

---

*The observed (H + 1)-hour gamma dose rate for fission products derived from the observed total gamma dose rate at H + 24 hours, assuming that 52% of the (H + 24)-hour gamma dose rate was due to tungsten [Knox, 1964b].

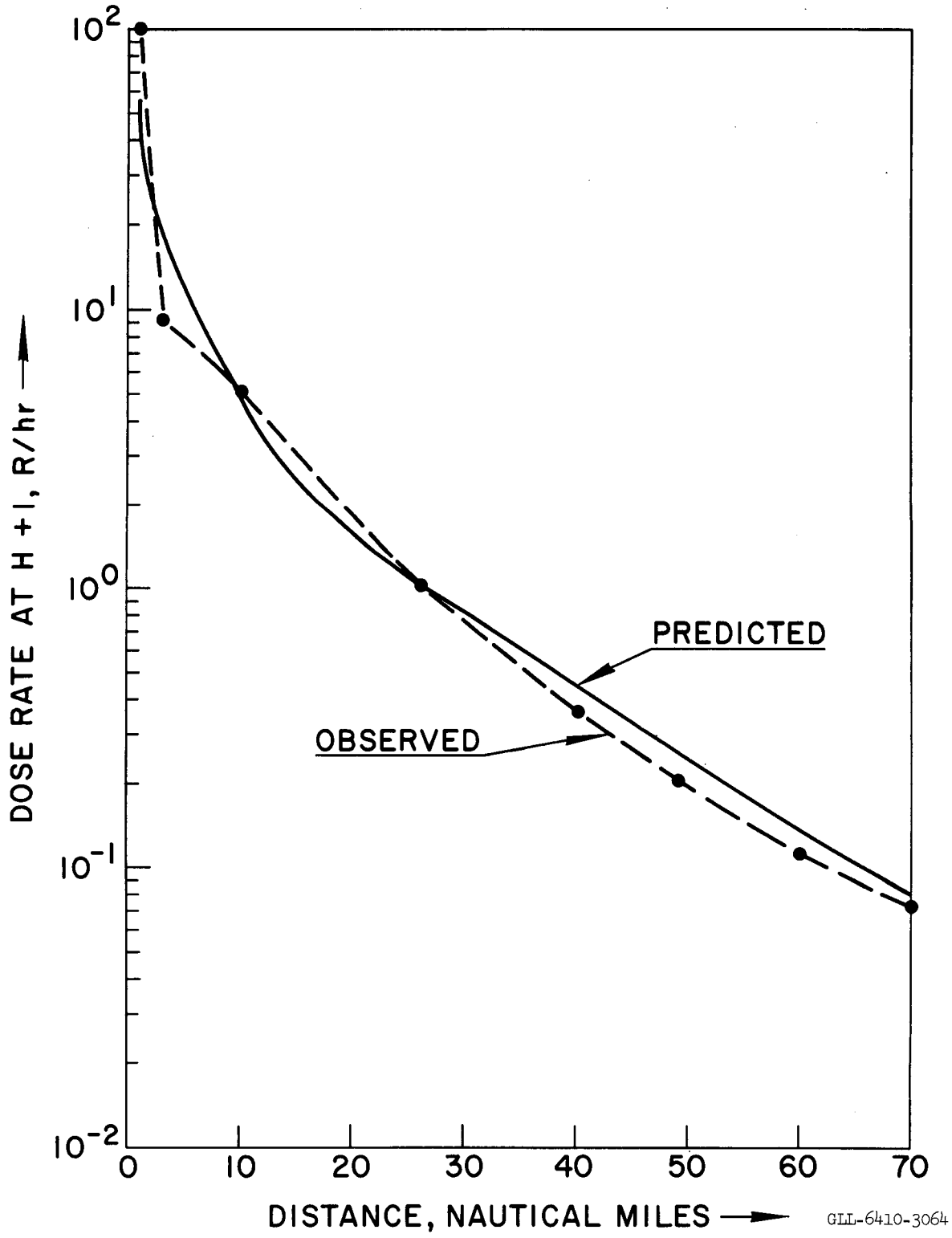


Fig. 6. The calculated and observed gamma dose rate at H + 1 hours as a function of distance along the hot line of the Sedan pattern (diagnostic calculation).

activity-particle size distribution parameters in order to duplicate the observed Danny Boy fallout pattern. In this event no visible main cloud was observed [Nordyke and Wray, 1964]. Thus in the diagnostic calculation with the cratering fallout model we assume that 100% of the $F_c$ gamma activity is in the base surge cloud, and a preliminary value of $F_c = 0.05$ is assumed. The activity-particle size distribution parameters determined in this calculation are given below:

$$w_b(1) = 0.9$$

$$w_b(2) = 0.1$$

$$\ln \bar{r}_b(1) = 3.0$$

$$\ln \bar{r}_b(2) = 5.7$$

$$\sigma_b(1) = 0.69$$

$$\sigma_b(2) = 0.59$$

Figure 7 shows the calculated (H + 1) dose-rate-vs-distance curve from the model, and the observed (H + 1) dose rate vs distance. As was previously mentioned, the value of $F_c$ used in the cratering fallout model calculation was 0.05; if the value of $F_c = 0.04$ (reported later, Nordyke and Wray [1964]) had been used, the agreement between the calculated (H + 1) dose rate and the observed (H + 1) dose rate vs distance would have been better than shown in Fig. 7.

Recently, effort has been expended to obtain machine capability of plotting the calculated (H + 1) dose rate patterns for an arbitrarily selected interval of dose rate. Figure 8 shows the machine-plotted dose rate pattern for the Danny Boy diagnostic calculation. The computer pattern breadth at 25 miles downwind is about 7 miles, and the breadth of the observed pattern at this distance is 5.5 miles. It should be noted that the closure of the isodose rate line of $10^{-4}$ R/hr at (H + 1) in the plotted pattern is artificial and is the

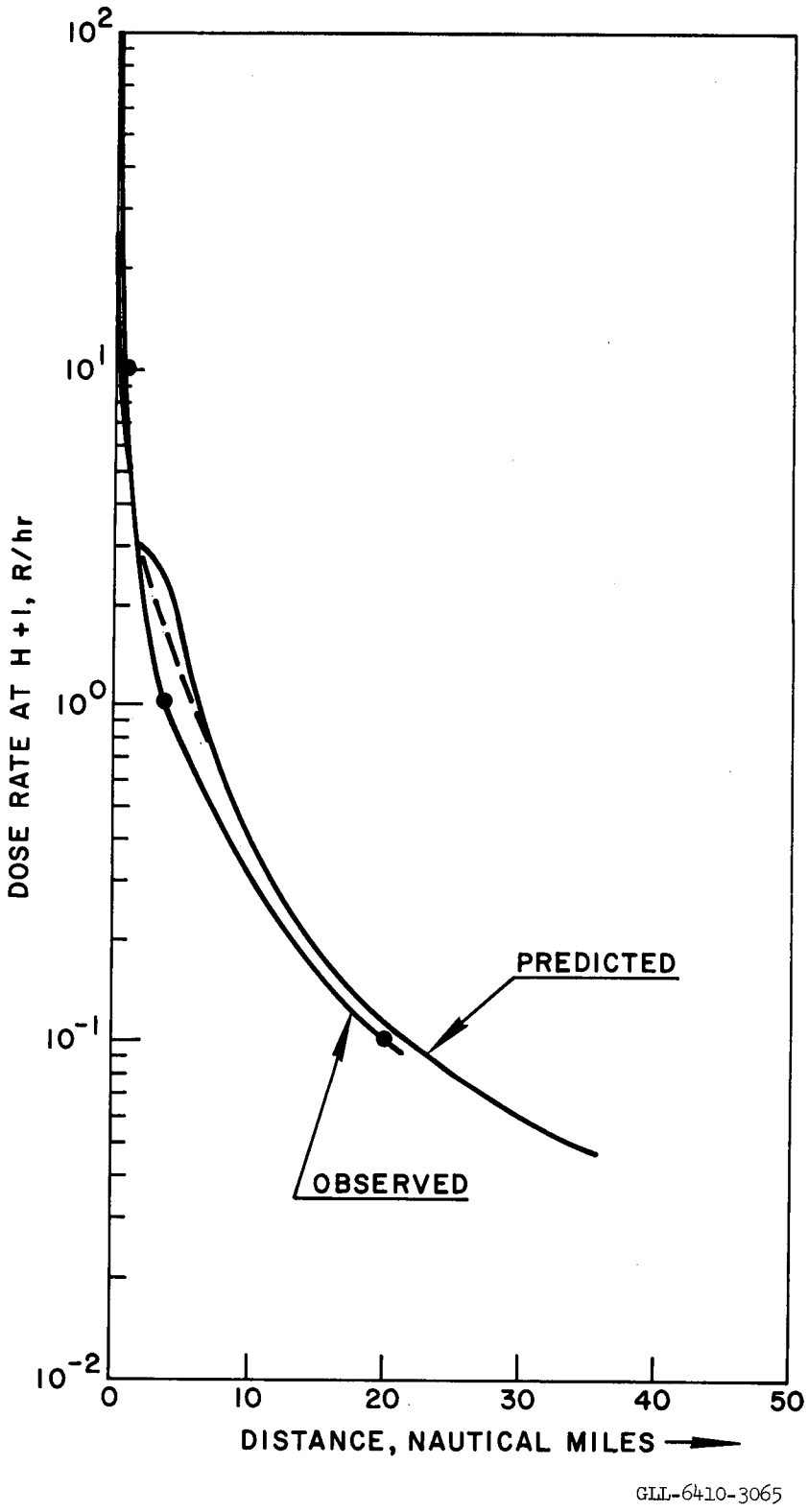


Fig. 7. The calculated and observed gamma dose rate at H + 1 hours as a function of distance along the hot line of the Danny Boy pattern (diagnostic calculation).

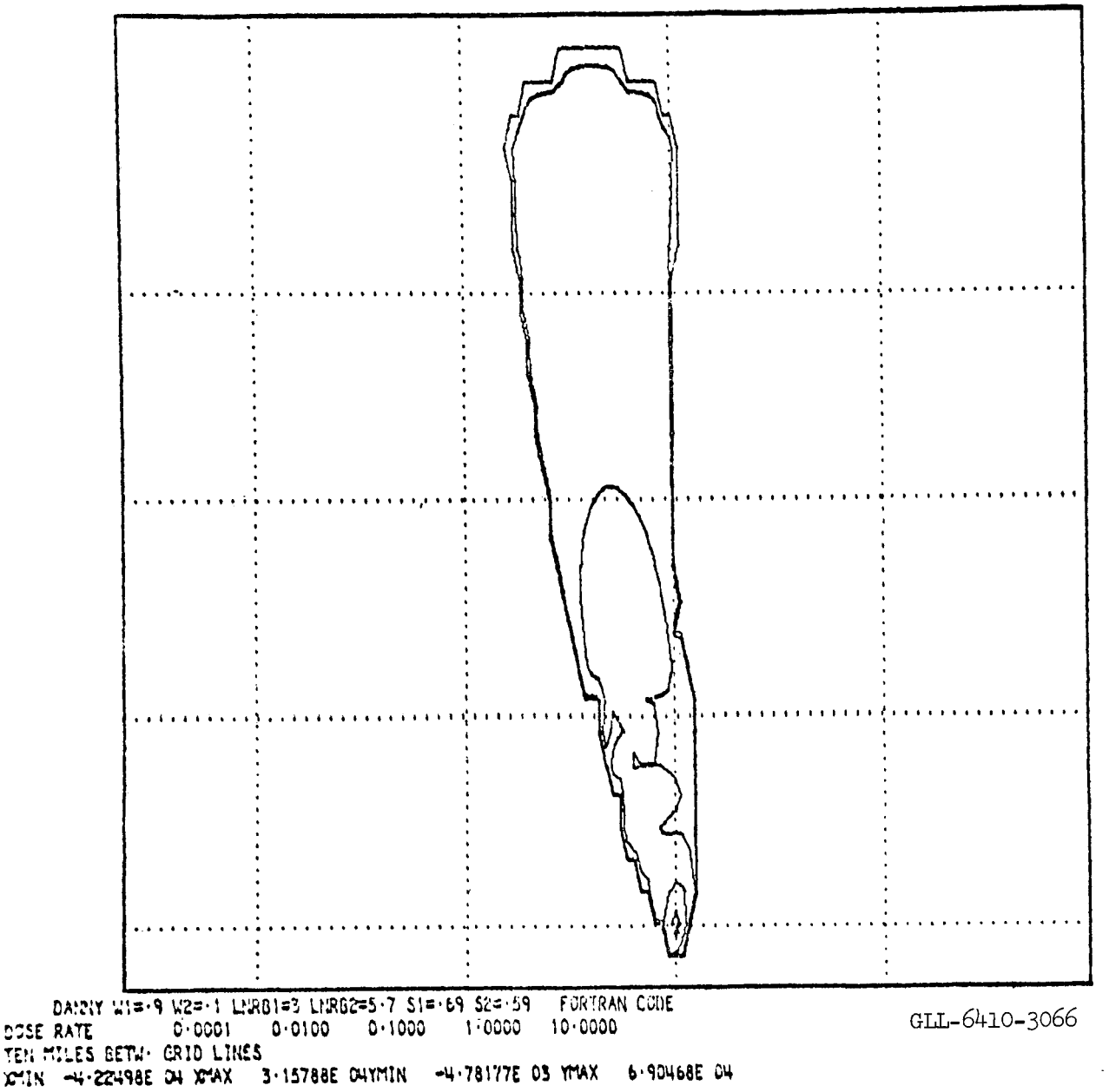


Fig. 8. The machine-plotted (H + 1)-hour gamma dose rate pattern for the Danny Boy event (diagnostic calculation).

result of the logic used for the computer plotting, rather than the result of the cratering fallout model. All isodose rate lines will apparently be closed at the downwind edge of the pattern if computed dose rate information is insufficient for their appropriate extension downwind. The observed (H + 1) gamma dose rate pattern for Danny Boy is shown in Fig. 9 for comparison with the computer-plotted pattern.

## V. INDEPENDENT TEST OF THE MODEL FOR TEAPOT ESS

An independent test calculation of the cratering fallout model (calibrated on Sedan) was performed using the Teapot ESS event. The observed winds at shot time, the observed cloud geometry, the published fission yield of 1.2 kt, and $F_c = 0.85$ (an early preliminary value of $F_c$) were input to the model. Figure 10 shows the calculated and observed (H + 1) gamma dose rate as a function of distance along the hot line of the pattern. A comparison of these two dose-rate-vs-distance curves shows that the largest error between calculation and observation is of the order of a factor of 2.5. An examination of the radiosonde observation (NTS) near shot time indicates that the vertical temperature distribution of the layer through which the particles were falling was slightly superadiabatic. Under such conditions, it is possible that the vertical eddy diffusion on the Teapot ESS shot day was larger than average. If enhanced vertical eddy diffusion were operative, the dose rate would be slightly less near ground zero and enhanced downwind.

Other model confirmation tests have been performed. These include calculations with the surface burst version of the model on the Apple II and Zucchini events [Knox, 1964a] and several other atmospheric events whose results remain classified at this date. The results of these additional tests were satisfactory.

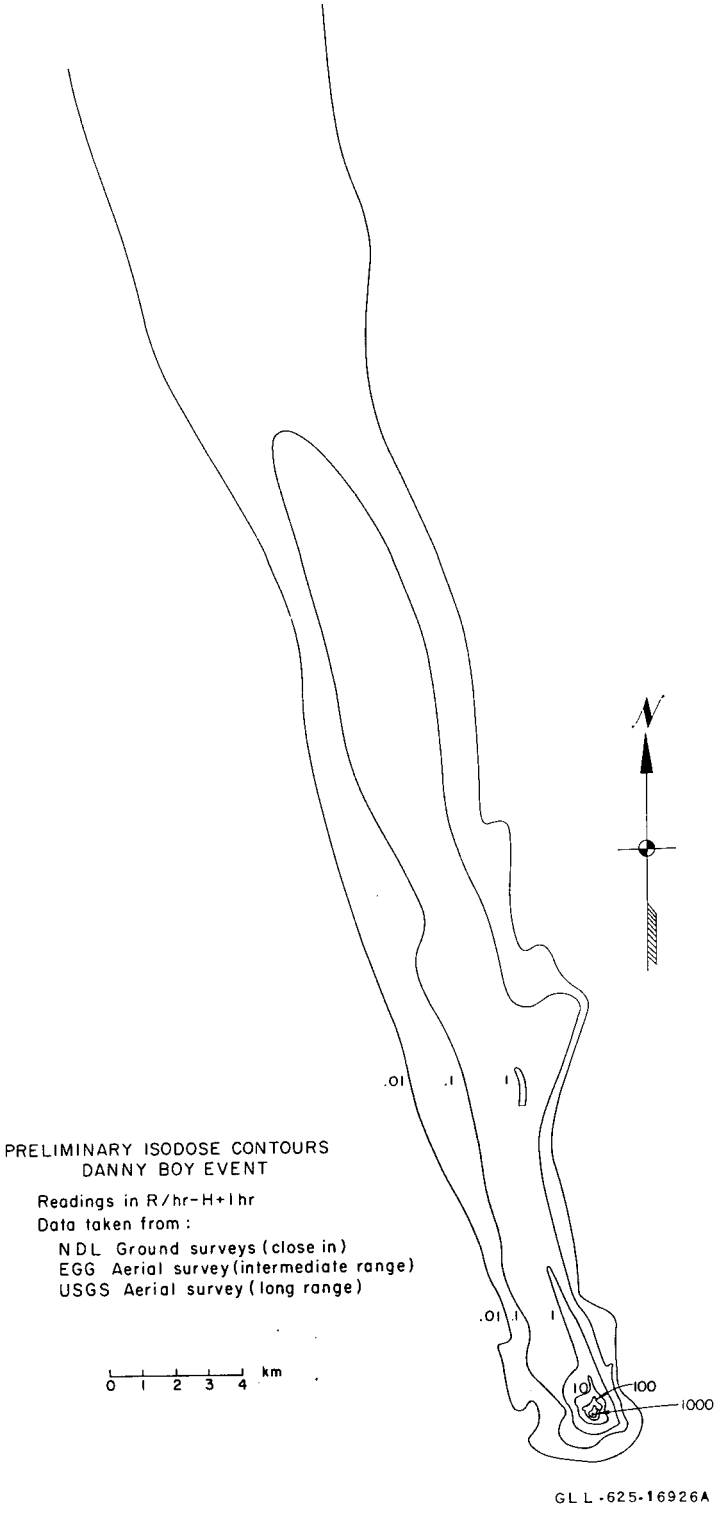


Fig. 9. Preliminary gamma isodose rate contours observed at H + 1 hours, from Nordyke and Wray [1964].

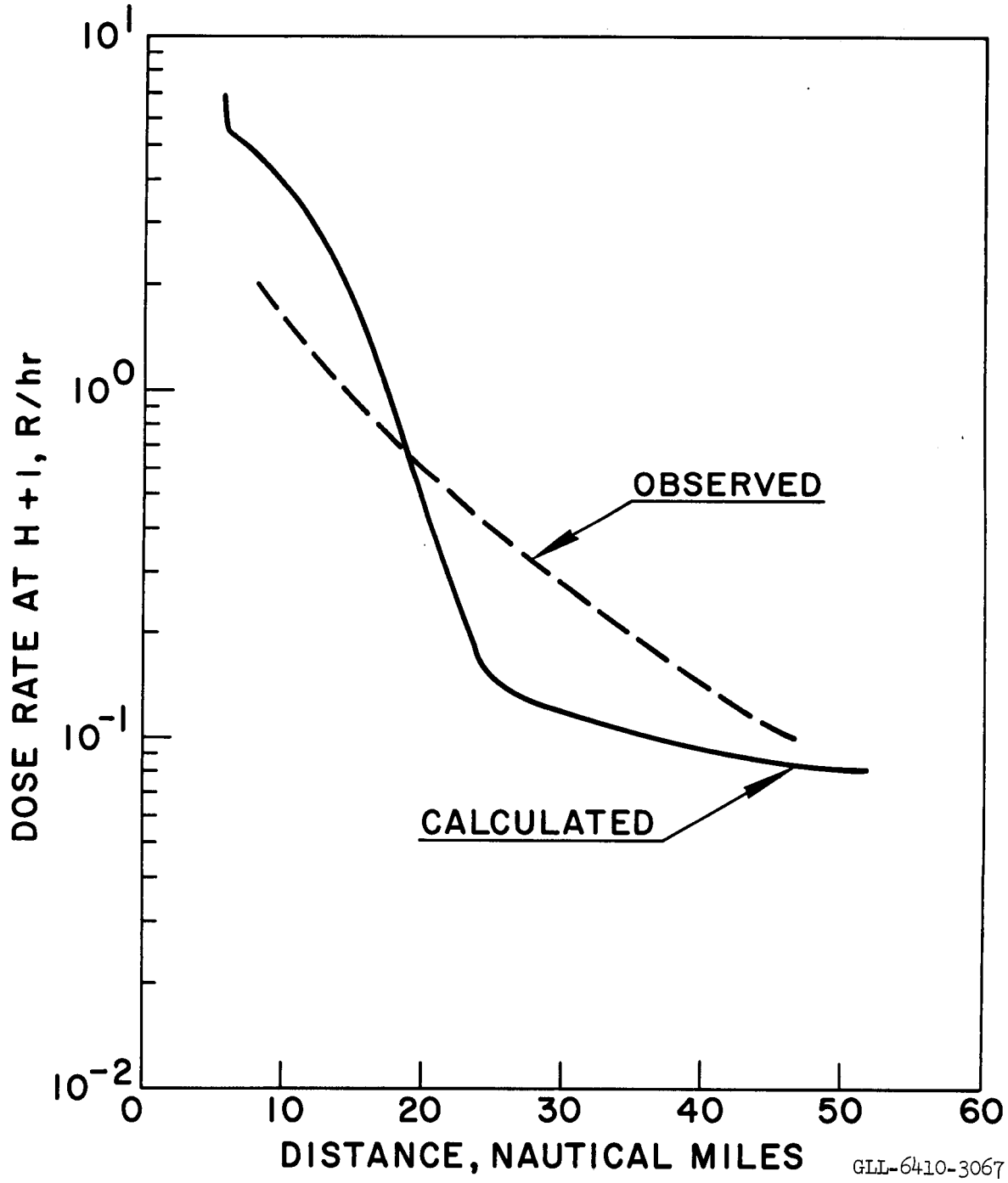


Fig. 10. The calculated and observed gamma dose rate at H + 1 hours as a function of distance along the hot line of the pattern (predictive calculation), Teapot ESS.

# VI. COMMENTS ON THE PREDICTION OF FALLOUT FROM ROW CHARGE EVENTS

In principle the fallout pattern from a row of subsurface nuclear detonations may be estimated with the cratering fallout model, provided the model input parameters are adequately known for row charge events. In the current state of knowledge, the cloud geometry input parameters and the value of $F_c$ appear to be the most difficult to specify. Study of time-lapse photography of the main cloud and base surge cloud evolution from past H. E. row-charge tests give significant experimental information on the cloud geometry parameters. For example, empirical methods of predicting crosswind radius and height of the base surge originating from H. E. row-charge events have been discussed [Knox and Rohrer, 1963]. In this latter study, it was shown that for five equal-weight charges, equally spaced and emplaced at the same depth of burial, the resulting base surge cloud has approximately the same radius as the base surge cloud from a large single shot of the same total yield and at the same scaled depth as the smaller charges. The base surge height for a 5-charge row event is approximated, reasonably well, by scaling the height of surge cloud for a single-charge event by the 0.2 power of the total yield of the row charge events.

A first approximation to the geometries of the individual main cloud may be obtained by treating each main cloud independently and estimating the cloud top and radius of the individual cloud from the work of Day [W. Day, U. S. Army Corps of Engineers Nuclear Cratering Group, LRL, private communication, 1964]. Examination of the H. E. row-charge documentary photographs of the Rowboat, Dugout, and pre-Buggy events indicates that such an approximation is reasonable. This approximation can, of course, be in error if main cloud interactions occur. There is a need to evaluate the uncertainty in

fallout prediction for multiple-charge events in cases where cloud interactions lead to the injection of radioactivity at levels higher in the atmosphere than predicted.

Concerning the $F_c$ for row charge events, preliminary experimental results for H. E. single and row-charge events have been reported previously [Graves, Wray, and Pierce, 1963]. In this study, results of the measured vented fraction of $La^{140}$ tracer from single and row-charge H. E. events were given. The experimental evidence suggests that the vented fraction from row-charge events may be about twice that for single-charge events. One of the more pressing needs for fallout prediction from row-charge events is the establishment, either through experiment or theory, of the dependency of the $F_c$ on yield, depth of burial, or charge spacing.

However, the development of computer aids for the row-charge fallout prediction problem can proceed independently of the solution of the two above-cited problems. To this end, the capability of plotting fallout patterns for multicloud and/or multidetonation events has been developed. Figures 11 and 12 show, respectively, the (H + 1) dose rate patterns computed for 10 Danny Boy detonations on an east-west line with charge centers separated by 33.5 meters, and 10 Danny Boy detonations on a north-south line with charge centers separated by 33.5 meters. For the purpose of these calculations, each detonation is assumed to vent 5% (e. g., $F_c = 0.05$), the individual clouds are assumed to be that of Danny Boy, and the input wind for each cloud fallout problem is assumed to be the shot time wind for Danny Boy. These two row-charge fallout patterns, although detectably different as determined from the printout, appear to be very similar. These calculational results suggest that the fallout pattern from a small-scale, row-charge event is not sensitive to the orientation of the wind to the alignment of the charges.

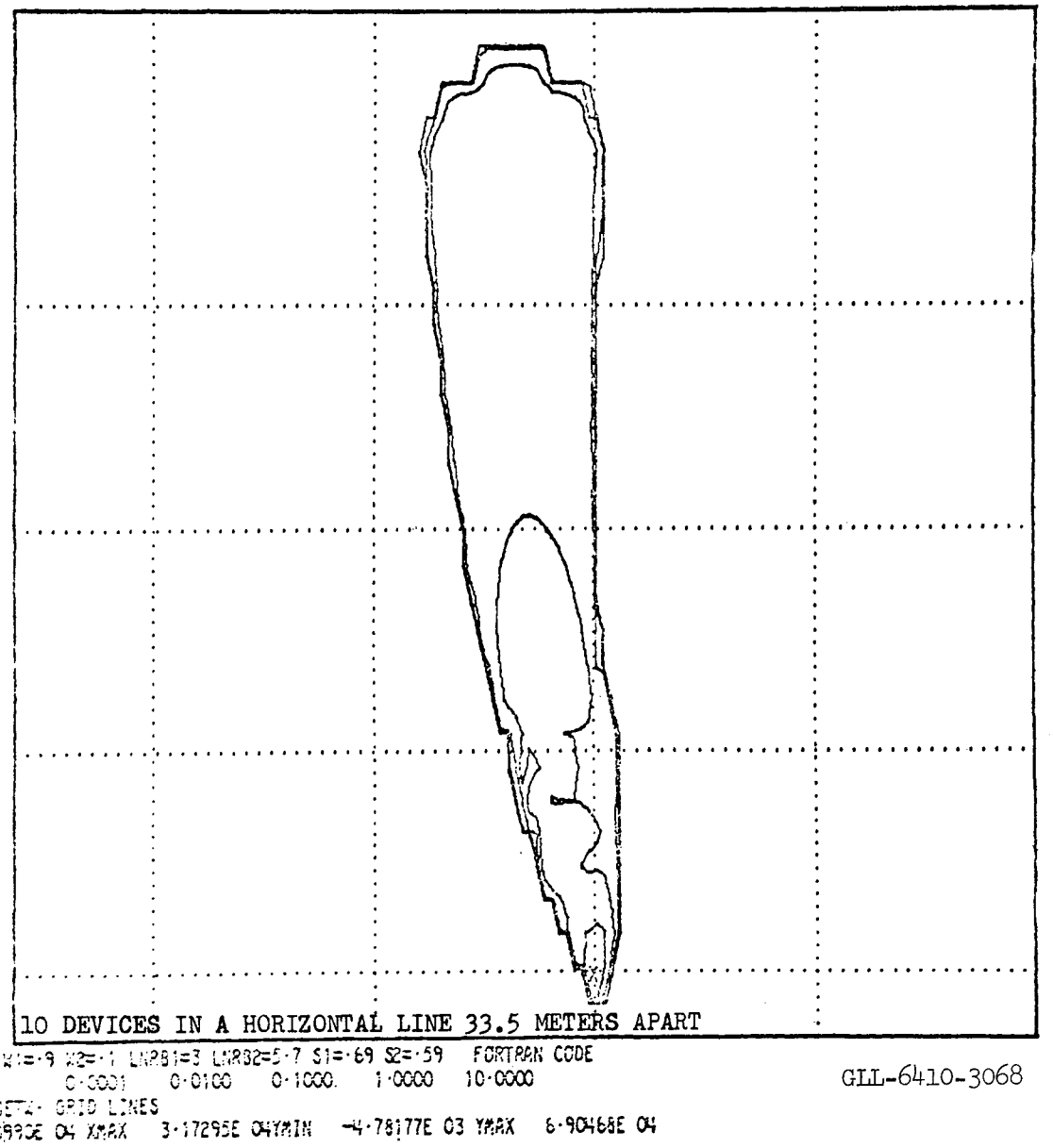


Fig. 11. The (H + 1)-hour gamma dose rate pattern computed for 10 Danny Boy detonations on an east-west line with charge centers separated by 33.5 meters.

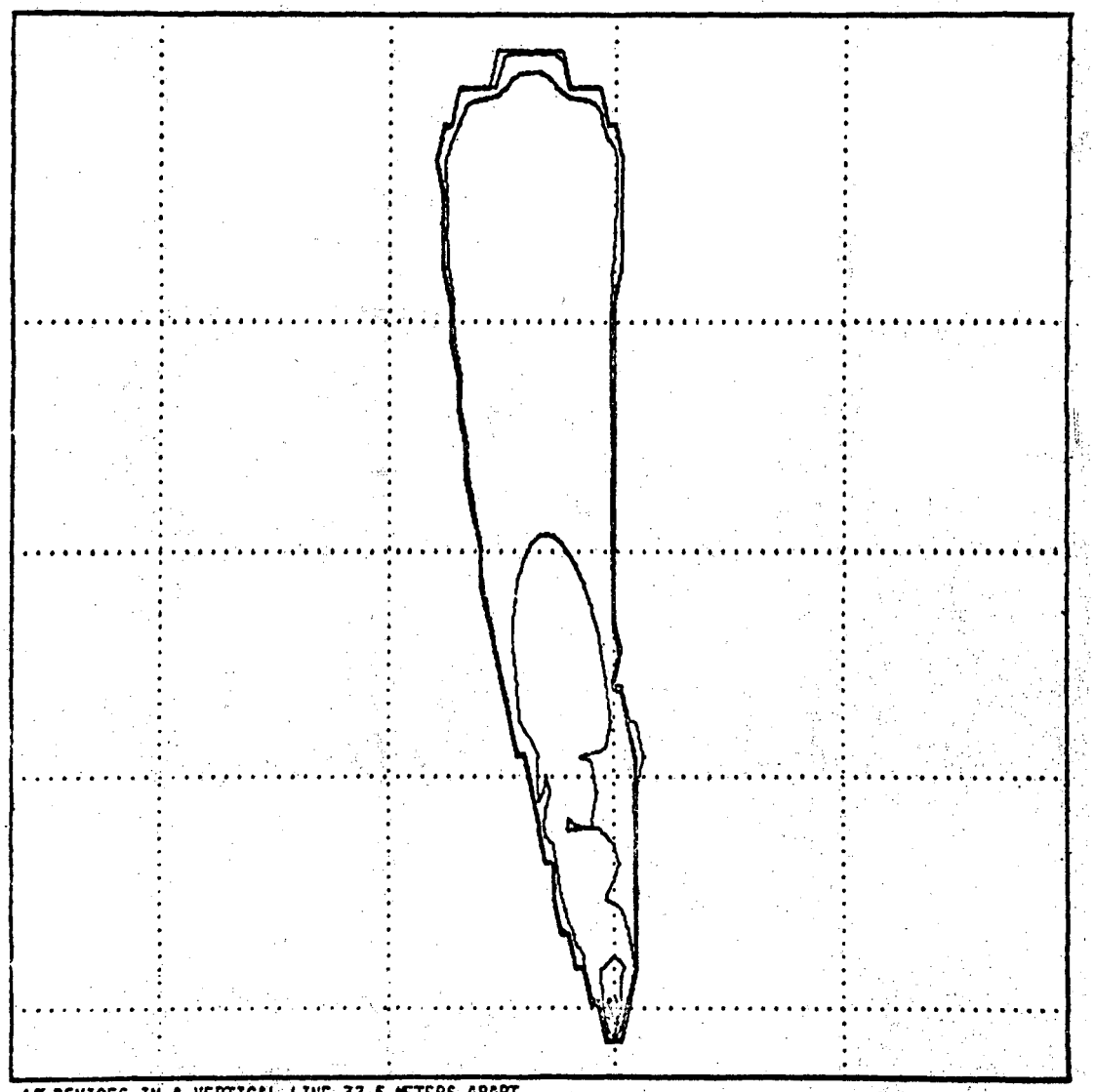


Fig. 12. The (H + 1)-hour gamma dose rate pattern computed for 10 Danny Boy detonations on a north-south line with charge centers separated by 33.5 meters.

## VII. CONCLUSIONS

In conclusion, it may be stated that the cratering fallout model developed gives reasonable results for the prediction of the area of the pattern, geometry of the dose rate contours, and (H + 1) dose rate vs distance along the hot line. The independent testing of the model should be extended to include more than the Teapot ESS case shown and the several others cited.

Meteorological improvements in the cratering fallout model could well include the following items: (a) the prediction of synoptic-scale changes in the normal and tangential shear components, (b) better understanding of the growth of the debris disks through horizontal eddy diffusion during their earthward fall, (c) the prediction of diurnal change of wind at low levels and close to ground zero, (d) the inclusion of the effects of topography on the evolution of the horizontal wind field, (e) the effect of terrain-induced circulations on fallout deposition, and (f) a better solution to the cloud rise problem for cratering detonations.

However, before embarking on the development of the above-cited meteorological improvements in fallout prediction, one must consider potential improvements which may come from other areas. Areas of promise are cratering physics and filtration theory for the vented-fraction problem, special emplacement for control of vented fraction, and the improvement of nuclear explosives.

Acknowledgments

The author wishes to acknowledge the interest often expressed by Dr. Gary Higgins and the late Dr. A. Vay Shelton in the work herein reported, as well as programming support given by Mrs. Leota Barr and Mr. Roger Fulton.

## REFERENCES

Batten, E. S., D. S. Inglehart, and R. R. Rapp, 1960. "Derivation of Two Simple Methods for the Computation of Radioactive Fallout," The RAND Corporation Rept. RM-2460.

Graves, E., W. R. Wray, and R. B. Pierce, 1963. "Scope of Chemical Explosive Cratering Experiment," U. S. Army Corps of Engineers Nuclear Cratering Group, Lawrence Radiation Laboratory, Livermore, Preliminary Rept. PNE-300.

Higgins, G. H., 1963. "Calculation of Radiation Fields from Fallout," Lawrence Radiation Laboratory, Livermore, Rept. UCID-4539.

Knox, Joseph B., 1964a. "The Prediction of Wind and Fallout," draft of presentation at the DASA-NRDL Fallout Symposium, Nov. 1962, Lawrence Radiation Laboratory, Livermore, Rept. UCID-4662.

Knox, Joseph B., 1964b. "Status Report on Cratering Fallout Models," Lawrence Radiation Laboratory, Livermore, Rept. UCID-4663.

Knox, Joseph B., and R. Rohrer, 1963. "Base Surge Analysis," Lawrence Radiation Laboratory, Livermore, Final Report for Project Pre-Buggy PNE-304.

McDonald, J. D., 1960. "Rates of Descent of Fallout Particles from Thermonuclear Explosions," J. Meteorol. 17, 380-381.

Nordyke, M. D., and W. Wray, 1964. "Cratering and Radioactivity Results from a Nuclear Cratering Detonation in Basalt," J. Geophys. Res. 69, 675-689.

Rapp, R. R., and J. D. Sartor, 1957. "Rate of Fall Through the Atmosphere of Irregularly Shaped Particles," The RAND Corporation Rept. RM-2006.

/sh